Dust Source Activation Frequency across East Asia

2 Lingle Chen^{1#}, Kerstin Schepanski², Anya J. Crocker¹, Chuang Xuan¹, Paul A. Wilson¹

- ¹School of Ocean and Earth Science, University of Southampton, Waterfront Campus, National Oceanography
- 4 Centre, Southampton, UK

1

10

11 12

13

14 15

16

17

18 19

20

21

22 23

24

25

26 27

28

29

30

31

32

33

34

35

36

37 38

39 40

41

42

- 5 ²Freie Universität Berlin, Department of Earth Sciences, Institute of Meteorology, Berlin, German
- 6 #Corresponding author:
- 7 Lingle Chen, School of Ocean and Earth Science, University of Southampton, Southampton, UK
- 8 Email: lingle.chen@soton.ac.uk

9 Abstract

Plumes of mineral dust in East Asia deleteriously impact the health and livelihoods of hundreds of millions of people in Mongolia, China, Korea, and Japan and perturb Earth's energy balance and climate. However, the sources of this dust are not well-documented, limiting understanding of dust emissions. Here, we systematically quantify dust source activation frequency (DSAF) across East Asia (80-130°E; 27-52°N) between January 2016 and December 2023. Our data reveal a vast dust-active area extending from the Tibetan Plateau in the southwest to the Huin Bair Sandy Land in the northeast, but two regions dominate: southern sources centred on the margins of the Taklimakan Desert and northern ones centred on the valleys of the Gobi Desert. East Asia is most dust-active in boreal spring (46% of all recorded events). This seasonal peak is pronounced in northern sources where snow cover, vegetation and orographic/topographic influence on winds are clear controls on DSAF. The main southern sources are active yearround with DSAF-hotspots attributable to desiccated lakes and riverbeds. The Tibetan Plateau, commonly considered a sink for in-bound windblown dust, is also a dust source, particularly in winter, with emissions controlled by precipitation patterns, snow cover and wind funnelling through deep river gorges. Contrary to suggestions, our data show that the Loess Plateau is not a major dust source. We document a marked increase in dust source activation during the 2020 extreme heat wave on the overgrazed Mongolian Plateau grasslands. Our data provide a framework to study past variability in the two-way climate interactions that control dust emissions on historical and geological timescales and a baseline from which to measure future change.

1. Introduction

The deserts of East Asia (figure 1) are a major supplier of mineral dust to the atmosphere (Ginoux et al., 2004), emitting between 400 and 1,000 teragrams (Tg) of dust annually (Kok et al., 2021), with serious impacts on the health and livelihoods of hundreds of millions of people in Mongolia, northern China, Korea, and Japan (Shao and Dong, 2006). Dust from East Asia is also transported vast distances to the North Pacific Ocean (Pye and Zhou, 1989), North America (Zdanowicz et al., 2006), and Greenland (Huang et al., 2015), influencing cloud physics, regional radiation budgets and climates (Huang et al., 2014). Yet the sources of this dust and the frequency of their activation have received less attention than atmospheric dust plumes and their transportation. Early studies of dust storm activity in East Asia used data from meteorological stations (Kurosaki and Mikami, 2003; Qian et al., 2002; Sun et al., 2001; Wang et al., 2005), the Total Ozone Mapping Spectrometer Absorbing Aerosol Index (TOMS AI) (Prospero et al., 2002) and dust emission modelling (An et al., 2018; Xuan and Sokolik, 2002).

Moderate Resolution Imaging Spectroradiometer (MODIS) data, with twice-daily observations, have been employed to study dust activity in the Taklimakan and Gobi deserts (Nobakht et al., 2021; Zhang et al., 2008, 2015a) and stereo imaging from the Multi-angle Imaging Spectro Radiometer (MISR) has been used to trace East Asian dust plume motion every 6-7 days (Yu et al., 2019). However, in data sets of such limited temporal resolution, dust transport in the atmosphere obscures the sources of these emissions and their activation frequency, thereby hindering assessment of mechanistic forcing.

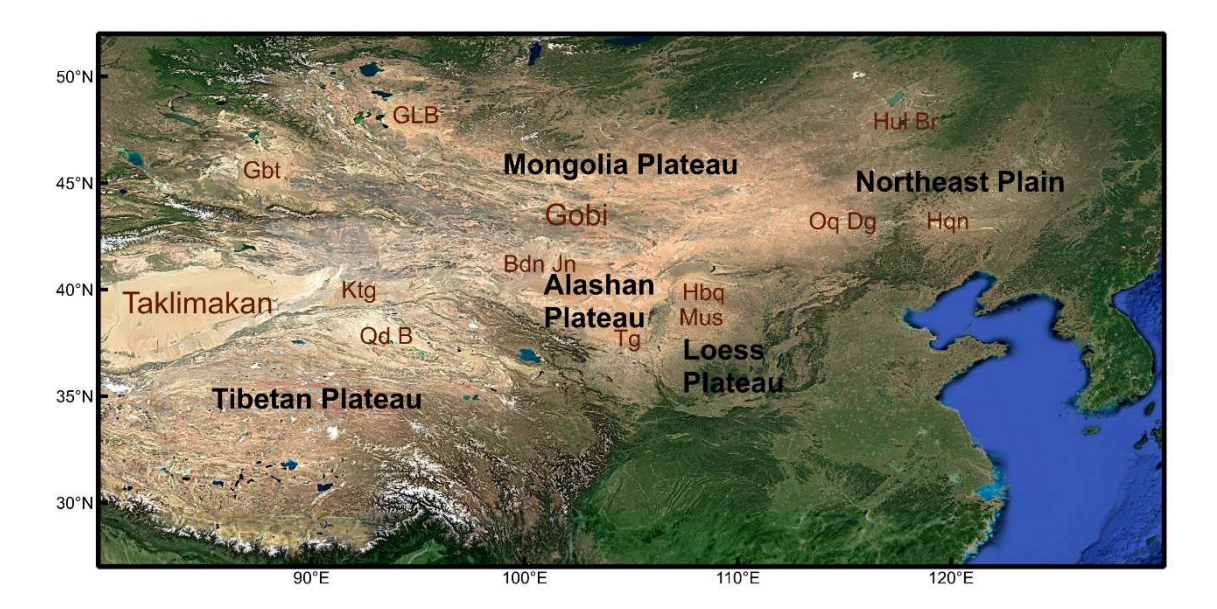


Figure 1. Study region with place names and geographic features mentioned in the text. Dust source active regions are labelled in brown, and highland/lowland regions are highlighted in bold black. Key locations include the Mongolian Plateau, the Alashan Plateau, the Loess Plateau, the Tibetan Plateau, and the Northeast Plain. The two primary dust source activation centres, the Taklimakan and the Gobi Deserts, are highlighted in brown. Secondary dust source regions include the Great Lake Basin (GLB), the Gurbantunggut Desert (Gbt), the Hulun Buir Sandy Land (Hul Br), the Onqin Daga Sandy Land (Oq Dg), the Horqin Sandy Land (Hqn), the Kumtag Desert (Ktg), the Baidan Jaran Desert (Bdn Jn), the Tengger Desert (Tg), the Qaidam Basin (Qd B), the Hobq Desert (Hbq), and the Mu Us Sandy Land (Mus). The base map is sourced from Google Earth ®.

A key advance in pinpointing dust sources was provided by the thermal infrared radiance data from the Metaset Second Generation (MSG) Spinning Enhanced Visible and InfraRed Imager (SEVIRI), which offers 15-minute temporal resolution and has been used to track dust emissions to their sources across North Africa (Schepanski et al., 2007), the Arabian Peninsula (Hennen et al., 2019), and the Horn of Africa (Kunkelova et al., 2024). For East Asia, the new-generation geostationary meteorological satellites Himawari-8/9 provide similar capabilities. The potential of this approach is demonstrated by studies of individual dust events originating from the Gobi Desert and northeastern China (Altausen et al., 2019; Kai et al., 2021) and the Taklimakan Desert (Yumimoto et al., 2019). However, a comprehensive assessment of dust source activity across East Asian is lacking.

Here, we utilize high-spatiotemporal-resolution dust RGB imagery from the Himawari-8/9

satellites to (i) present the first detailed high-resolution DSAF record of East Asia (80–130°E,

73 27–52°N); (ii) examine the seasonality of East Asian dust source activations; and (iii) evaluate

74 the land surface conditions that promote dust source activation.

2. Methodology

75

80

83

84

85

87

88

89

90 91

92

93

94 95

96

97 98

99

100

101

102

104 105

106

107 108

109

High-resolution spatiotemporal remote sensing satellite data from Himawari-8/9 were used to

77 identify dust source activation from January 2016 through December 2023 (8 years).

Himawari-8/9 is a new-generation geostationary meteorological satellite launched by the Japan

79 Meteorological Agency (Bessho et al., 2016). Himawari-9 began its backup operations for

Himawari-8 in March 2017 and officially took on the primary operational role in December

81 2022. The Advanced Himawari Imager (AHI) sensor aboard these platforms features 16

wavelength bands (channels): channel 1–3 image in the visible part of the spectrum, channel

4–6 the near-infrared, and channel 7–16 the far-infrared wavelength bands. The geospatial

monitoring range of Himawari-8/9 is from 85°E to 160°W and from 60°N to 60°S. The spatial

resolution is $2 \text{ km} \times 2 \text{ km}$ (up to 0.5 km per pixel in the visible spectrum), and the temporal

86 resolution is 10 minutes over East Asia.

We applied the Dust RGB method to convert Himawari-8/9 far-infrared channels to dust composite images (Akihiro, 2020). This method takes advantage of the difference in reflection and transmission characteristics between atmospheric dust and other substances (e.g., low/mid/high-level cloud, and cold/warm deserts). Three infrared channels, i.e., 11, 13, and 15 are processed as follows: red (BT15–BT13), green (BT13–BT11), and blue (BT13). Areas with bright magenta or pinkish shading are recorded as dust, tan-brown colours as clouds, and light cyan or light green as warm or cold deserts (supplementary figure 1). Smoke is not detected by dust RGBs because they use only IR bands. While dust and volcanic ash may appear similar in RGB, our study region is not an active volcanic zone or under the influence of advected volcanic ash plumes. Areas that emit dust were identified visually and marked as dust source activation events on a 1° × 1° gridded record covering East Asian deserts, spanning 80–130°E, 27-52°N. We generated 420,768 dust composite images covering an 8-year period (January 2016 to December 2023) and grouped them into 2,922 daily animations to enable rapid manual identification of dust plumes. We tracked 21,829 individual dust plumes (pinkish shading in the animation) back to their points of origin. Manual identification and calculations of DSAF follow the method of Schepanski et al. (2007):

103
$$DSAF (\%) = {\binom{N_s}{N_D}} \times 100$$

 N_s = total number of days with at least one dust event in 1° × 1° grid cell within a given interval,

 N_D = number of days of available satellite observation within the same interval.

Note that DSAF indicates the timing and frequency but not mass flux of dust emissions. Dust source identification is not possible under optically thick clouds or atmospheric dust layers. The pink shading of dust varies with surface emissivity, atmospheric moisture, atmospheric

dust concentration and dust layer altitude (Banks et al., 2019). Manual dust source identification necessarily introduces the potential for human error but, while we anticipate future improvements in automated algorithms, for now, skilled humans introduce fewer inconsistencies in their analyses of DSAF (AlNasser and Entekhabi, 2024). To minimize subjective bias, we followed the protocol of Schepanski et al. (2012) wherein all dust plumes were recorded but the modest subset (~3% of total events) with an obscured source (e.g., because of cloud cover), were classified as uncategorized and excluded them from our analysis to ensure a conservative and reliable estimate of dust activations.

3. Results and Discussion

3.1 Spatial and Seasonal Characteristics of East Asian Dust Source Activation

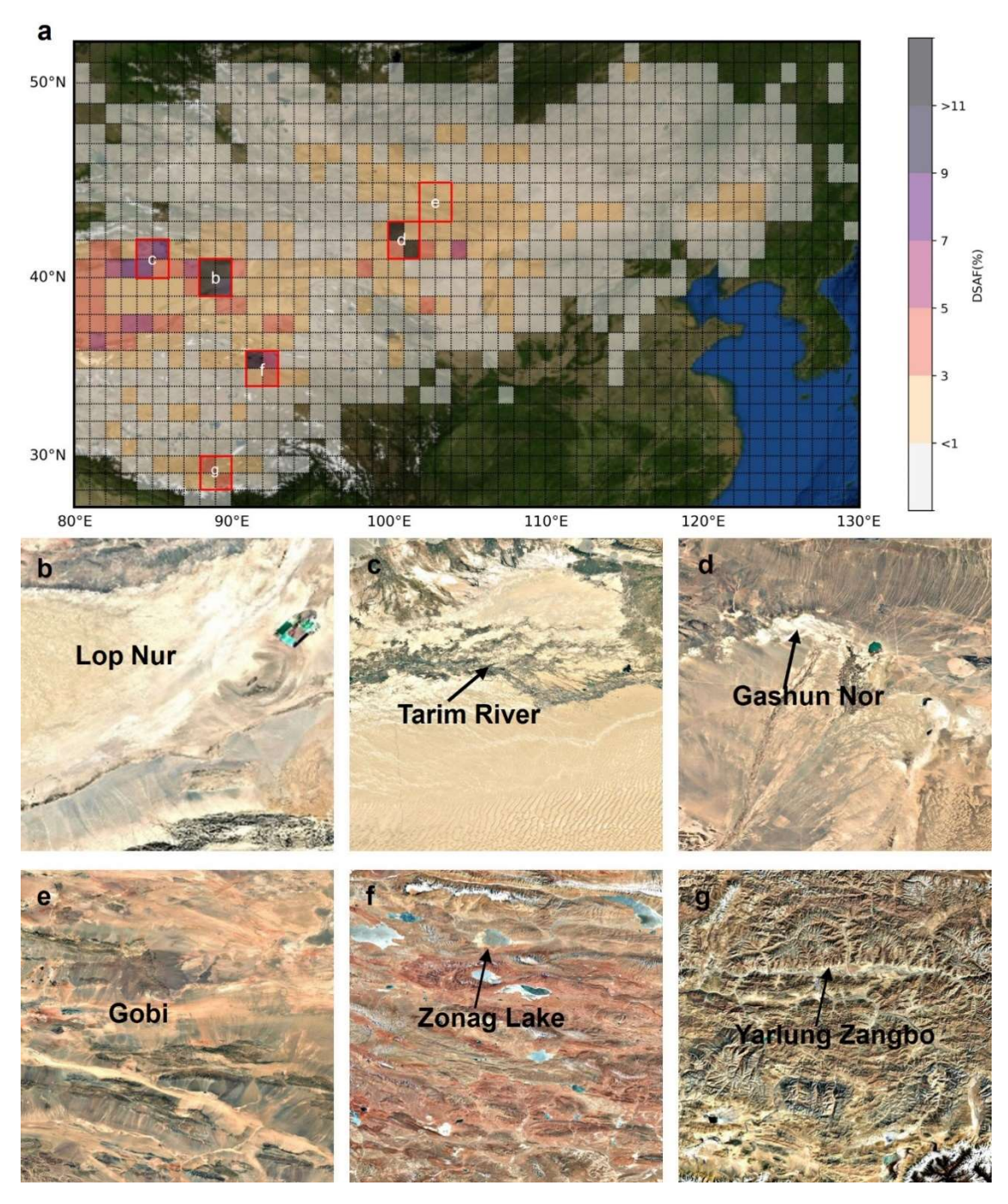
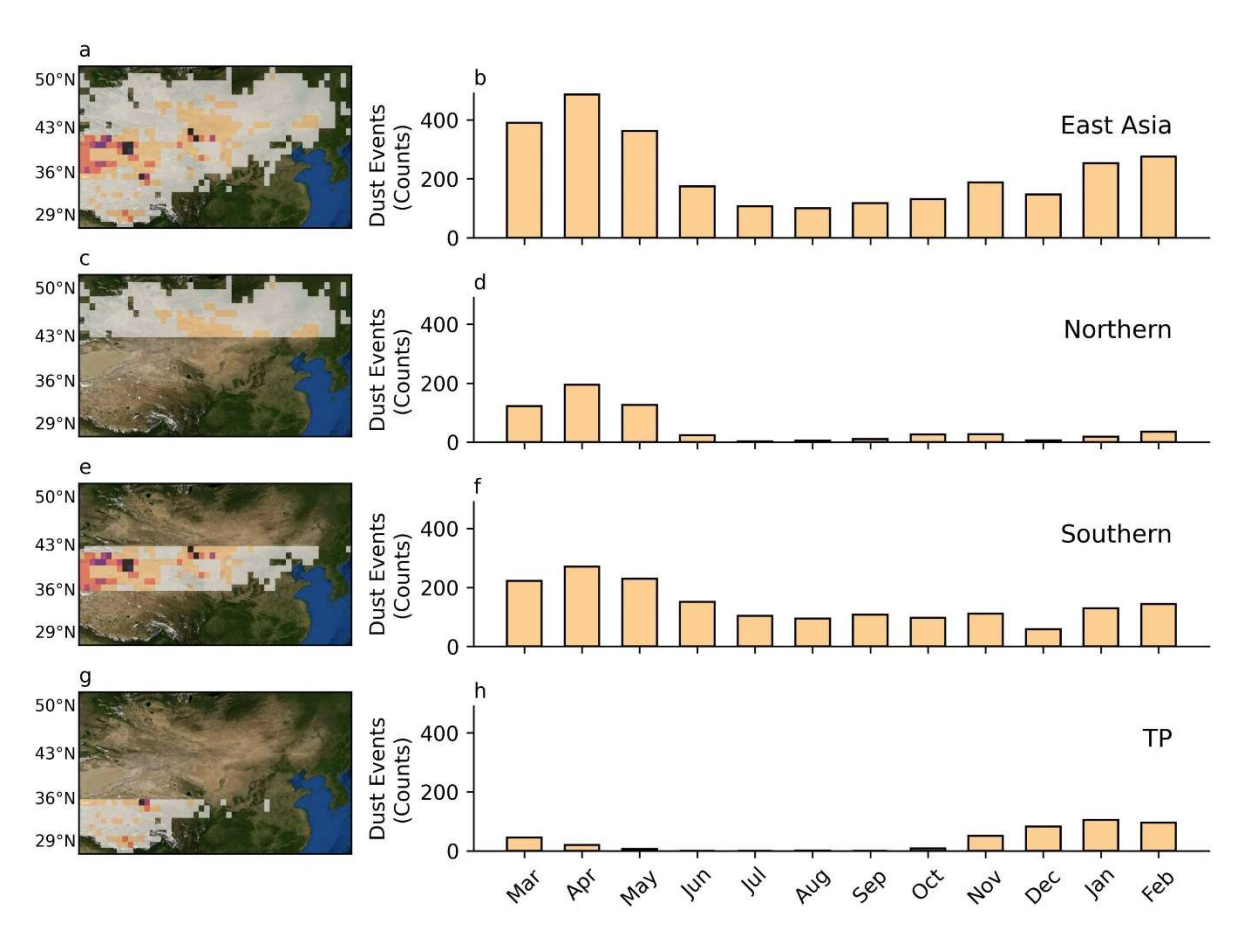


Figure 2. (a) Average annual dust source activation frequency (DSAF) from 2016 through 2023. The intensity of the colour represents the DSAF percentage (darker shades = higher DSAF values). The small red (solid-line) boxes around areas of high DSAF indicate the full extent of the land surface images shown in panels b-g.

Our data reveal a vast area that is dust-active, extending from the Tibetan Plateau in the southwest to the Hulun Buir Desert in the northeast, and we identify two primary regions: a northern one, centred on the Gobi Desert and a southern one, centred on the Taklimakan Desert (figures 1 and 2(a)). This result supports some interpretations from smaller data sets and model simulations (Ginoux et al., 2012; Kim and Lee, 2013; Prospero et al., 2002; Xuan et al., 2004; Zhang et al., 2008), but the spatial and temporal granularity in our data permits precise identification of sources and mechanistic insight into dust generation. East Asia is most dust active in spring (46% of all events recorded) and least active in summer (14%) (figure 3(a-b)). We divide these two main source regions along 43 °N, roughly corresponding to the southern limit of Mongolian Plateau (figure 3). The northern region is most-active in spring (figure 3(d)) while the southern one, sandwiched between the Tibetan Plateau and Mongolian Plateau, 36°N-43°N (figure 3(e)), is dust-active year-round (figure 3(f)). We also identify the Tibetan Plateau (figure 3(g)) as a dust source, mostly active in winter and early spring (figure 3(h)). However, contrary to many suggestions (Xuan and Sokolik, 2002; Xuan et al., 2004) and in support of the opposing view (Kurosaki and Mikami, 2003; Lim and Chun, 2006), we show that the Loess Plateau is not an active present day dust source (figures 4 and 5).



121

122

123 124

125 126

127

128

129130

131

132

133

134135

136

137

138 139

140

- 142 **Figure 3.** Monthly distribution of dust source activation (counts) for (a) East Asia (80–130°E;
- 143 27–52°N), (b) the northern source region (north of 43°N), (c) the southern source region
- 144 (36°N–43°N), and (d) the Tibetan Plateau (TP, 27°N–36°N).
- 145 A seasonal and latitudinal shift in atmospheric dust in East Asia has been inferred based on data
- from sparsely distributed meteorological stations (Han et al., 2008). Our data show that, for
- half of the year (summer and autumn), the East Asia dust activation belt is centred on ~40°N,
- in the southern source region (figure 4). In spring, high DSAF values extend to higher latitudes
- incorporating northern sources (figure 4(b)) where regional wind speeds also peak in spring
- 150 (Shao and Dong, 2006). In winter, the highest DSAF values are found at lower latitudes
- including the Tibetan Plateau (figure 4(h)), implying the influence of the prevailing westerly
- jet over the Tibetan Plateau (Schär et al., 2009).
- 153 In spring, in addition to the Taklimakan and Gobi deserts, other northern sources, such as the
- 154 Great Lake Basin, the northern Mongolian grasslands, and the Northeast Plain, also contribute
- to dust emissions (figure 4(a)). The Great Lake Basin on the northwestern Mongolian Plateau,
- home to one of the largest dune fields on the Mongolian Plateau, interconnected lakes, wetlands,
- and semi-arid landscapes (Lehmkuhl et al., 2024), produces dust on ~3% of spring days (figure
- 158 4(a)), a contribution that has not been clearly quantified before. Eastern Kazakhstan and the
- 159 Gurbantunggut Desert also peak in dust source activation during spring, serving as minor
- 160 contributors (figure 4(a)). This finding is consistent with the analysis of Nobakht et al. (2021)
- who used twice-daily MODIS imagery, but we document more dust events in East Kazakhstan
- and the Gurbantunggut Desert during non-spring months. In summer, the highest DSAFs are
- observed around the margins of the Taklimakan Desert (figure 4(b)), and the Alashan Plateau
- is a secondary source (figure 4(c)). During autumn, the Taklimakan Desert and the Alashan
- Plateau remain the dominant dust sources, but activation frequencies are lower (figure 4(e)). In
- winter, dust source activation events are primarily concentrated on the Tibetan Plateau,
- 167 followed by the Taklimakan Desert, the Alashan Plateau, the Qaidam Basin and the Ordos
- Plateau, which includes the Hobq Desert and the Mu Us Sandy Land (figure 4(g)).

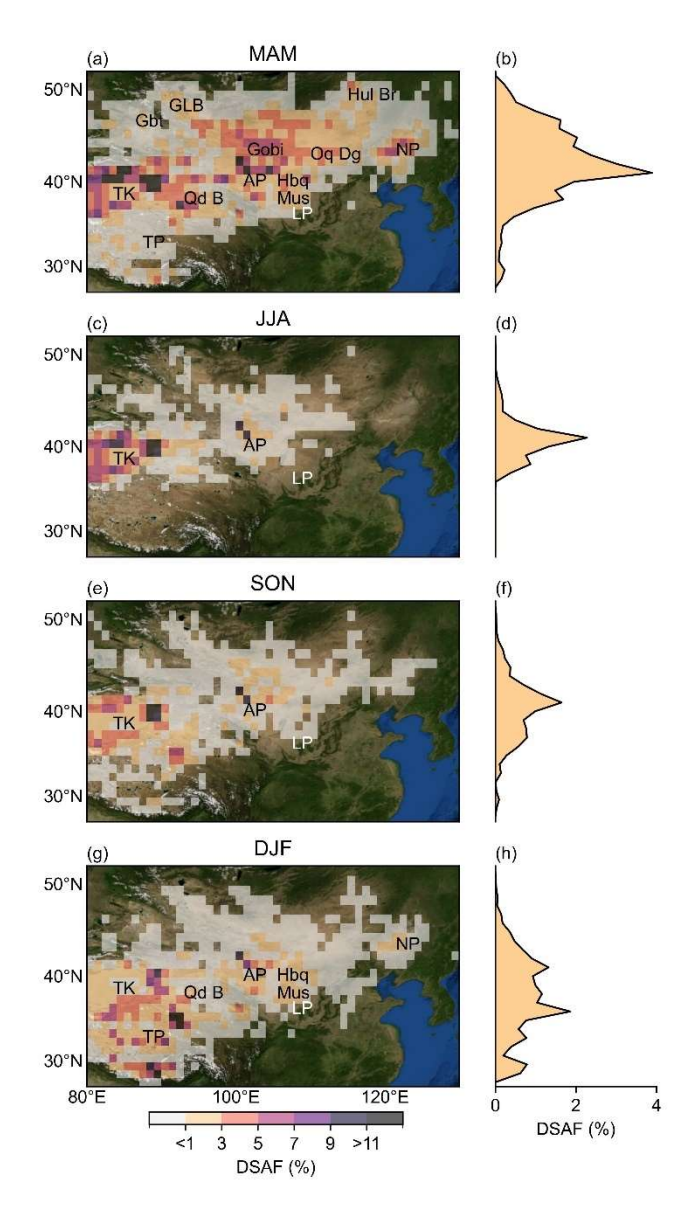


Figure 4. Seasonal latitudinal distribution of dust source activation frequency: (a-b) Spring (MAM, March, April, May), (c-d) Summer (JJA, June, July, August), (e-f) Autumn (SON, September, October, November), and (g-h) Winter (DJF, December, January, February). These frequencies are calculated from the recorded years between 2016 and 2023. Dust source regions labelled in black including: the Taklimakan Desert (TK), the Gobi Desert, the Great Lake Basin (GLB), the Gurbantunggut Desert (Gbt), the Hulun Buir Sandy Land (Hul Br), the Onqin Daga Sandy Land (Oq Dg), the Qaidam Basin (Qd B), the Hobq Desert (Hbq), the Mu Us Sandy Land (Mus), the Alashan Plateau (AP), the Tibetan Plateau (TP) and Northeast Plain (NP). The Loess Plateau (LP) is also indicated (in white because our data show that it is largely inactive, also see Figure 5).

3.2 Land Surface Drivers of Dust Source Activation

3.2.1 Dust Hotspots in the Taklimakan and Gobi Deserts

The highest DSAFs in East Asia occur in the southern source region, in the northeastern Taklimakan Desert (figure 1), especially around Lake Lop Nur (figure 2(b), 89°E, 40°N), where

184 dust activation occurs on ~19% of days (figure 2(a)). This result is consistent with findings derived from the twice-daily MODIS imagery Nobakht et al. (2021). While the date and cause 185 of Lop Nur's desiccation are debated (Dong et al., 2012), our data show that it is a hotspot of 186 dust activity (figure 2(b)). The Tarim River and associated floodplains, located on the northern 187 188 rim of the Taklimakan Desert (figure 2(c), 80–90°E, 40–41°N) is also a significant dust source with activation on \sim 7% of days (figure 2(a)). Glacial- and snow-melt from the Tianshan 189 Mountains are responsible for nearly 50% of annual river flow in the region (Chen et al., 2006). 190 191 The sediment transported during peak flow (summer ablation season) accumulates in loose, 192 dry soils along the riverbanks making them highly susceptible to wind erosion when river levels fall prior to the next summer ablation season (Rittner et al., 2016). Our data also show notable 193 dust source activation along the southern rim of the Tarim Basin (80–85°E, 36–37°N, ~6% of 194 195 days), including the Hetian River (80–82°E, 36–41°N, ~4% of days), which has not been 196 clearly identified as an active dust source before (figure 2(a)). These rivers, fed by glacial- and 197 snow-melt from Kunlun Mountains, deposit sediment in alluvial fans, terminating in the central 198 basin, where they desiccate during the dry season (Rittner et al., 2016).

199 The most active area in the northern dust source region of East Asia is the southwestern Mongolian Plateau in the Gobi Desert (figure 1, 98–105°E, 42–45°N) where dust activation 200 averages about 3% of days annually (figure 2(a)). The valleys of the Gobi-Altai Mountain 201 202 ranges (figure 2(e), 100–103°E, 43–45°N) exhibit the highest DSAF, reaching ~6% of spring 203 days (figure 4(a)) across a landscape rich in lakes and paleolake remnants (Lehmkuhl et al., 2018), which serve as abundant sources of fine-grained particles, readily mobilized by strong 204 winds. This region is also characterized by orographic convergence and topographic funnelling 205 206 of synoptic winds, triggering dust events associated with the passage of Mongolian cyclones 207 (Kai et al., 2021).

3.2.2 The Alashan Plateau: A Year-Round Dust-Active Source

208

The Alashan Plateau (98–106°E, 38–42°N) and its adjacent regions, in western Inner Mongolia 209 210 (northern China) (figure 1), is reportedly a source of dust storms (Sun et al., 2001; Wang et al., 211 2011; Xuan and Sokolik, 2002) but, until now, its complex landscape with altitudes ranging 212 from 820 m to around 1,500 m, deserts including the Badain Juran Desert, the Tengger Desert 213 and the Ulan Buh Desert, degraded oases and dried riverbeds (figure 5) made it challenging to discriminate dust sources (Wang et al., 2019). Our data show that the Alashan Plateau is dust-214 active throughout the year (figure 5). Dust activation occurs on ~3% of days (figure 5), peaking 215 in spring (~9% of spring days) (figure 3(c-d)) and desiccated water bodies are a key control. 216 217 The southern side of the Altai Mountains, particularly dry riverbeds in the Heihe Alluvial Plain (figure 5, 100–102°E, 41–42°N) and desiccated lakes such as Gashun Nor (dried in 1961) and 218 Sugu Nor (dried in 1992) are suggested to be dust-active (Kurosaki and Mikami, 2003; 219 Natsagdorj et al., 2003; Wu et al., 2016; Zhang et al., 2008). Our data reveal that Gashun Nor 220 221 (figure 2(d), 100 °E, 42°N) is the most dust-active source anywhere on the Alashan Plateau and 222 the second most active source in all of East Asia, with ~14% of days being dust-producing 223 (figure 5) including ~23% of spring days (figure 4(a)). The oasis areas along the Hexi Corridor 224 (97–102°E, 38–41°N) are also important contributors with dust activation on ~4% of days 225 (figure 5) and \sim 8% of spring days (figure 4(a)). Detrital materials from the Qilian Mountains

are transported by fluvial systems to the Hexi Corridor, supplying sediments that are well-suited for dust activation (Zhang et al., 2022). Spring ploughing of croplands in these oasis regions leads to bare land with loosened surface sediments, reducing the threshold frictional velocity needed to trigger dust emission (Shen et al., 2005).

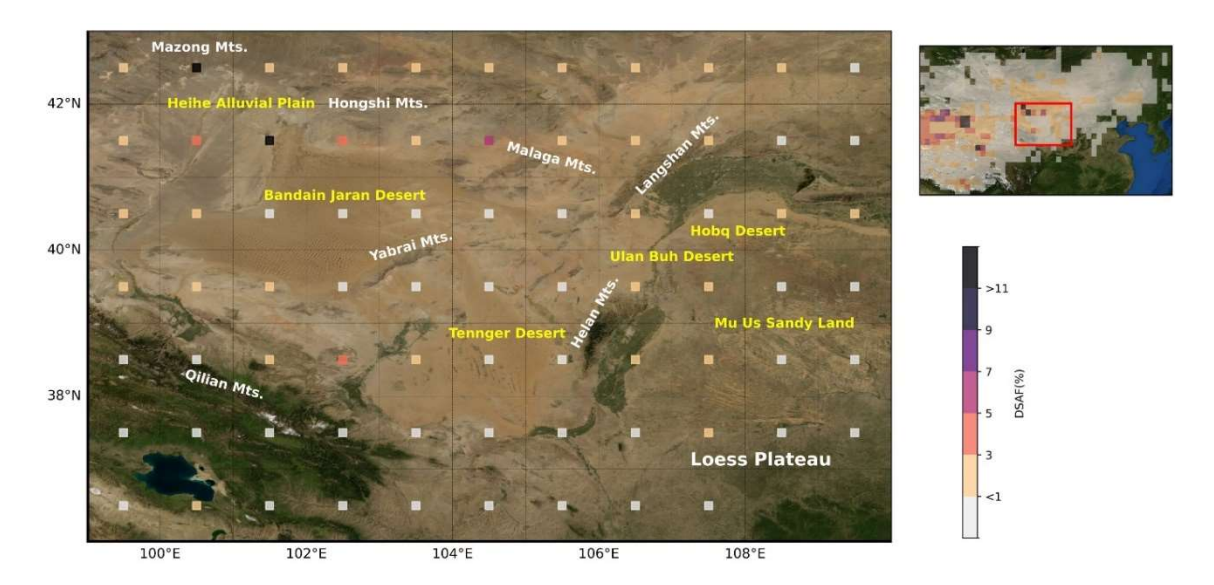


Figure 5. Annual dust source activation frequency (DSAF) on the Alashan Plateau and adjacent regions (see inset for location). DSAF for individual grid squares is shown as coloured mini pixels. Dust active regions (i.e., deserts, sandy land, dry lakebeds) are labelled in yellow. Mountains (Mts.) and plateaus are labelled in white. The underlying image is from NASA's Blue Marble: Shaded Relief.

The sandy deserts on the Alashan Plateau (e.g., the Badain Jaran Desert and the Tengger Desert) and the Ordos Plateau (e.g., the Hobq Desert and the Mu Us Sandy Land) are much less dust-active (<1% of days) (figure 5). This result (i) suggests that interpretations from detailed case studies (Luo et al., 2020; Wang et al., 2021) are regionally applicable and (ii) is consistent with findings from North Africa (Schepanski et al., 2007) and Arabia (Hennen et al., 2019; Kunkelova et al., 2022). We attribute it to a paucity of fine-grained sediments in these landscapes. Famously, the Chinese Loess Plateau is a sink for windblown dust transported from elsewhere, but its role as a dust source is debated (Kurosaki and Mikami, 2003; Xuan et al., 2004). Our data show it to be a negligible modern day dust source (figure 5), a result we attribute to dense vegetation coverage and soils with high clay contents that promote aggregation and clodding (Xuan and Sokolik, 2002).

3.2.3 The Mongolian Plateau and Northeast Plain

Spring Snow Cover and Vegetation

The Mongolian Plateau and adjacent regions (90–125°E, 43–52°N) exhibit pronounced seasonal variation in dust storms, vegetation and snow cover (Lee and Kim, 2012). Vegetation increases surface roughness, reducing wind speeds and roots bind soil particles, making them less likely to be entrained (Zender et al., 2003). Snow inhibits dust emissions by blanketing potential dust source areas, by increasing the threshold wind velocity required for dust emission

and by enhancing soil moisture after snowmelt (Kurosaki and Mikami, 2004; Tanaka et al., 2011). Our direct identification of dust sources enables a more precise evaluation of the role of snow cover and vegetation in modulating the spatiotemporal evolution of dust activation.

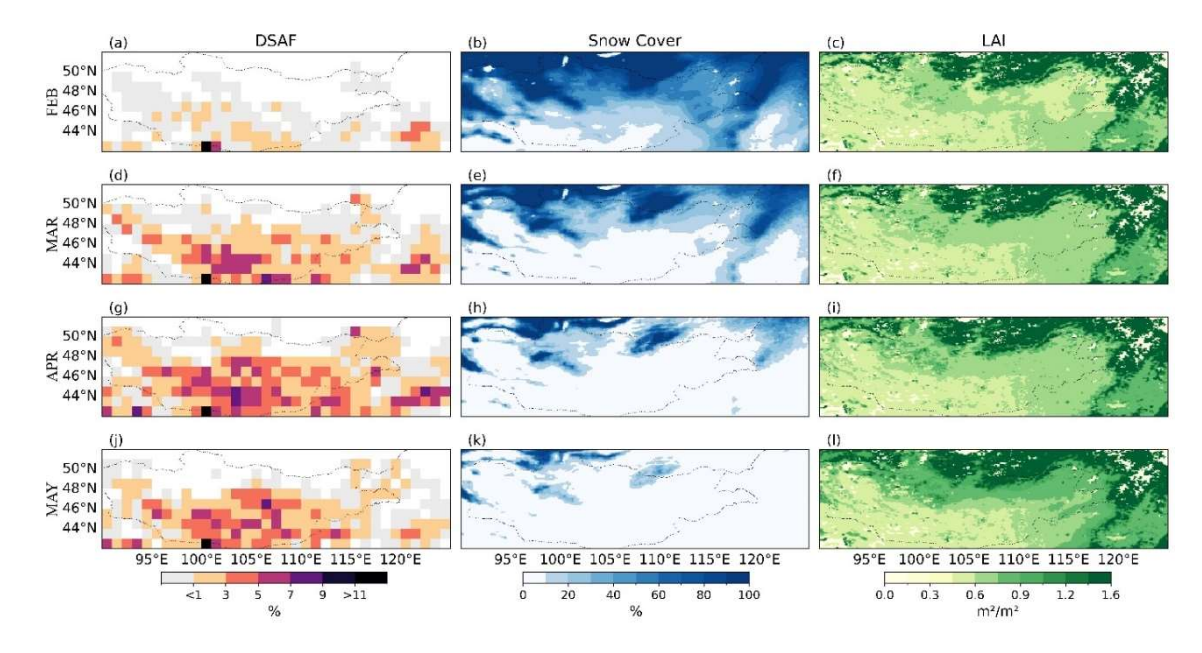


Figure 6. Dust source activation frequency (DSAF, left), snow cover (middle), and leaf area index (LAI, right) for the transition from winter to spring: February (FEB, a-c), March (MAR, d-f), April (APR, g-i), and May (MAY, j-l). Snow Cover and LAI index are reconstructed from European Centre for Medium-Range Weather Forecasts Reanalysis 5 (ERA5) data (average for 2016-2023).

The Mongolian Plateau experiences a pronounced dust storm season that begins in February, intensifies during March and April, and diminishes by May (Hao et al., 2024). Our data show that DSAF is minimal in February (<3% the month's days) across the Mongolian Plateau especially on its northern margin where extensive snow cover persists (figures 6(a-b)). Vegetation is limited in spring, but as snow gradually melts and retreats northward from February to April, DSAF increases significantly, peaking at 5-7% of days in the month (figures 6(c-i)). In May, despite the absence of snow cover, the resurgence of vegetation in the northern and northeastern parts of the Mongolian Plateau leads to a significant decline in DSAF down to 1–3% of the month's days (figures 6(j-l)). From 2016 to 2023 (February–May), Dust source activation events (>1%) occurred when LAI ranged from 0.5 to 1.0, with snow cover below 20% (Supplementary figure 2).

Human Land Use Change

Global dust mass loading is suggested to have increased by ~55% since pre-industrial times, with Asian dust contributing significantly to this change (Kok et al., 2023). However, current climate models fail to reproduce this increase, at least in part because they underestimate the influence on dust emissions of human-induced land use change which has been extensive in East Asia, especially on the Mongolian Pleau and the Northeast Plain (Ginoux et al., 2012). Today, the Mongolian Plateau and adjacent regions are characterized by three main land cover types: bare lands in the southwest, grasslands in northeast and croplands in the east (figure 7).

Our data show that the highest DSAFs are observed on bare lands on the southern Mongolian Plateau (activation on 3~5% of days during the first half year) (figure 7(a)). The grasslands that lie immediately to the north, in central-eastern Mongolia, are also recognized as both a natural dust source area (Shinoda et al., 2010) and, increasingly, as an area experiencing frequent droughts, leading to a reduction in vegetation cover and soil moisture (Nandintsetseg et al., 2021) and grassland degradation driven by overgrazing by growing livestock populations (Nandintsetseg and Shinoda, 2015). Our data show a spike in DSAF in this region during the first half of 2020 (figures 7(b-c)), the time of the record-breaking Siberian heatwave when the Verkhoyansk weather station recorded a daytime maximum of 38°C on June 20th, the highest temperature ever recorded north of the Arctic Circle with abnormally warm temperatures extending onto the Mongolian Plateau (Ciavarella et al., 2021). Furthermore, areas exhibiting a 2020-heatwave positive DSAF anomaly show higher livestock numbers compared to those with a negative 2020-heatwave DSAF anomaly (p-value = 0.037, Figure 7(d)). These observations strongly suggest a human-induced land-surface control on the DSAF anomaly during the first half year of 2020 involving grazing-induced grassland degradation during extreme heatwave conditions.

282

283

284285

286

287

288289

290

291

292293

294

295

296297

298299

300

301

302

303

304

305

306

Land use on the Northeast Plain is a mix of sandy lands (e.g., the Horqin Sandy Land, the Onqin Daga Sandy Land and Hulun Buir Sandy Land, figure 1), grasslands and croplands (figure 7a). Cropland extent has grown rapidly in northeast China in recent decades (Li et al., 2004) and field studies suggest that these black soil croplands are a source of dust storms (Zhang et al., 2015b). Our data support this suggestion, showing dust activation on ~7% of spring days (figure 4(a)), presumably driven by strong winds in the ploughing season.

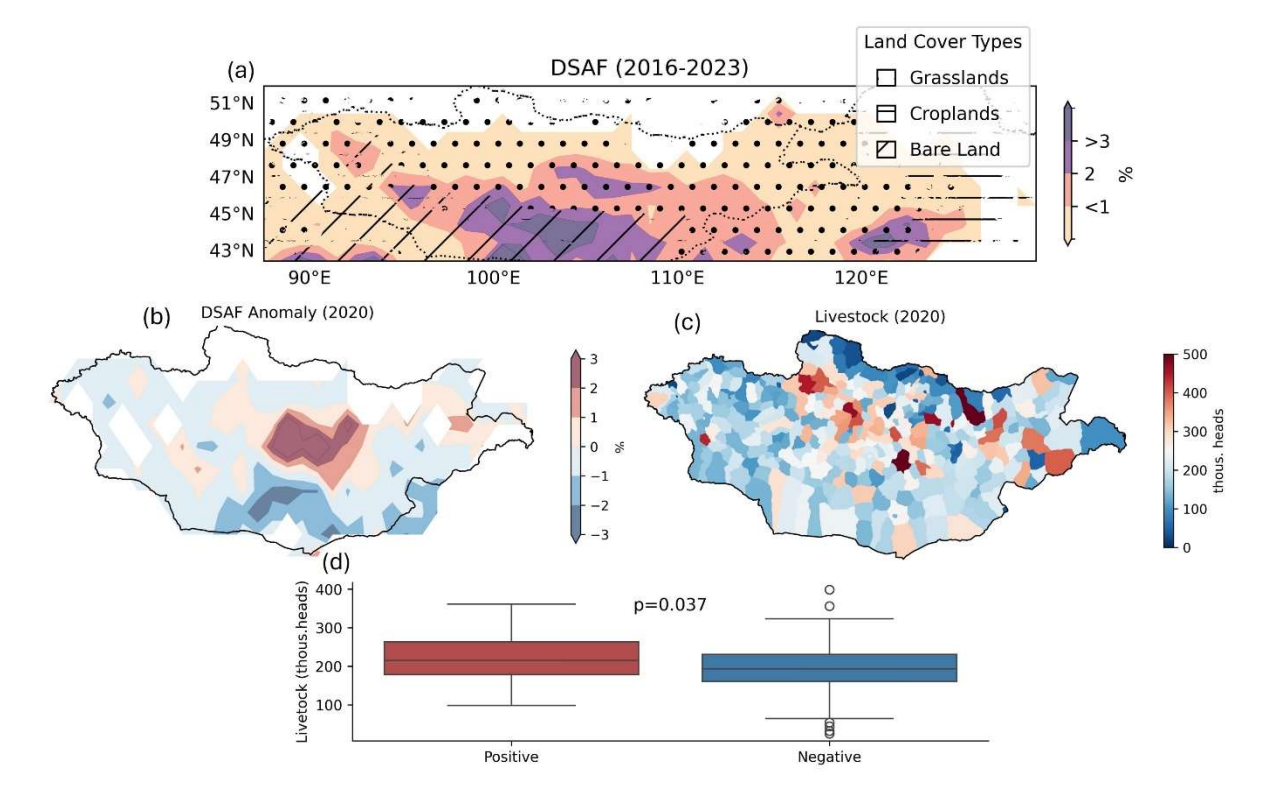


Figure 7. Response of Dust Source Activation Frequency (DSAF) to the extreme Siberian heatwave from January to June 2020. DSAF is shown in color (our data) and overlain with the

- average land cover (symbols) derived from MODIS MCD12C1 Version 6.1 data. Panel (a)
- displays DSAF from 2016-2023, panel (b) shows the 2020 anomaly (2020 minus the mean for
- 309 2016 through 2023), panel (c) shows livestock numbers in Mongolia for 2020 (the National
- 310 Statistical Office of Mongolia, https://www.1212.mn/), panel (d) compares livestock numbers
- 311 to the 2020 DSAF anomaly, with the t-test p-value shown in black. All panels use DSAF data
- 312 for the January-June period, the time frame during which the 2020 heatwave was most strongly
- 313 developed.

3.2.4 The Tibetan Plateau: A Winter-Early Spring Dust Active Source

- 315 The Tibetan Plateau is commonly regarded as a sediment sink for dust transported from
- 316 elsewhere, but it is also suggested to act as a dust source (Zhang et al., 2023), such as the
- 317 Yarlung Zangbo River Valley (Yang et al., 2025). Recently, however, dust emissions from
- 318 interior sources on the Tibetan Plateau have been suggested to be comparable to those of
- 319 northern China, with both areas suggested to produce approximately 130 Tg of dust annually
- 320 (Du et al., 2022). In our data, the Tibetan Plateau accounts for approximately 15% of all
- 321 recorded dust events across East Asia, with average activation rates <1% of days with the
- remaining 85% of dust events occurring in northern China (i.e., our northern and southern
- source regions), with average activation rates of 1% and 3% of days, respectively (figure 2(a)).
- Our data show that winter into earliest spring (i.e., December-March) is the primary dust
- season on the Tibetan Plateau (figure 3(g-h)). We identify three principle Tibetan Plateau dust
- sources (figures 8(a-b)): (i) the northern Tibetan Plateau (80–94°E, 35–37°N, covering the
- 327 northern part of the Changtang Plateau, the Hoh Xil Plateau, and the Qaidam Basin), with dust
- activation average at ~5% of winter days; (ii) the central Tibetan Plateau (80–93°E, 31–35°N,
- 329 including the Ali Valley between Changtang Plateau and Gangdise Mountains), with activation
- average at ~3% of winter days; and (iii) the southern Tibetan Plateau (82–93°E, 28–30°N,
- as especially the Yarlung Zangbo River Valley), with an activation on ~8% of winter days.

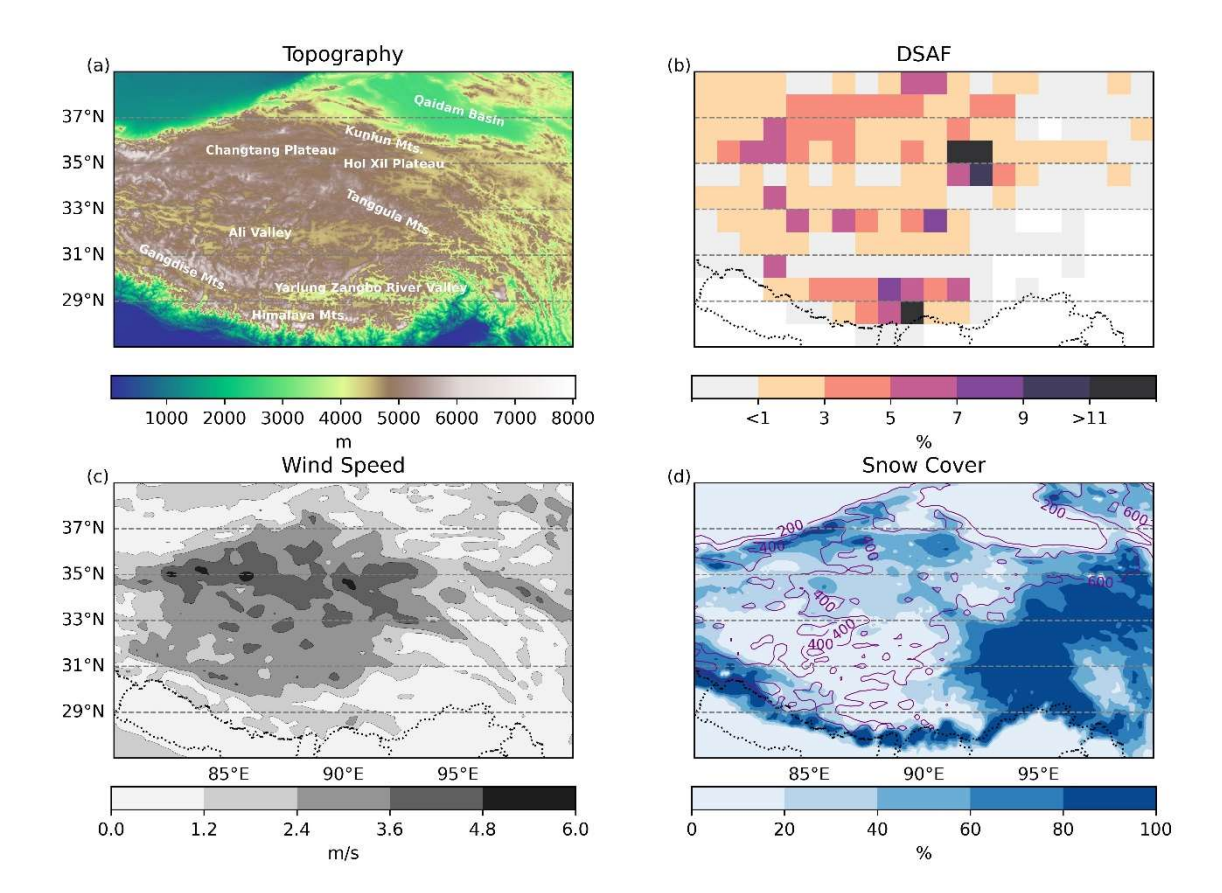


Figure 8. Controls on winter dust source activation frequency (DSAF) on the Tibetan Plateau. (a) Topography with mountain ranges and valleys labelled in white. (b) winter DSAF, (c) winter wind speed distribution and (d) winter snow cover distribution with annual precipitation in purple contour, all averaged over the study period (2016–2023). Snow cover, wind speed and precipitation are reconstructed from European Centre for Medium-Range Weather Forecasts Reanalysis 5 (ERA5) data (average for 2016-2023).

One exceptionally dust-active hotspot in the northern Tibetan Plateau source is Zonag Lake (figure 2(f)) on the Hoh Xil Plateau (activation on ~27% of winter days) (figure 8(b)). Here, extreme precipitation in 2011 triggered a flood that led to extensive erosion and deposition of a large sediment-rich area that is now exposed and an active dust-source (Lu et al., 2020b). The flood also caused thermal alteration of the freeze-thaw cycle, the melting of ground ice, and the destabilization of soil in the downstream region (Lu et al., 2020a). These processes accelerated permafrost degradation and increased the potential for dust emissions.

The topography of the Tibetan Plateau influences DSAF, with high DSAFs observed in lowelevation depositional environments such as the Ali valley (activation on ~3% of winter days) and Yarlung Zangbo River Valley (activation on ~8% of winter days) (figures 8(a-b)) because these basins generally act as depositional environments (Zender et al., 2003). From northwest to southeast, winds weaken while precipitation and snow cover both increase (figures 8(c-d)), leading to decreasing DSAF from the Changtang Plateau (figure 8b) toward the southeast, closely resembling the modelled dust flux distribution (Du et al., 2022). Extreme topographic variation in the Yarlung Zangbo River Valley, one of the world's deepest river gorges with depths reaching up to 5,000 meters, also contributes to the very high DSAF values recorded

- here. During winter, river levels fall, exposing sandbanks and floodplains (Yang et al., 2025)
- and the narrow and deep morphology of the valley helps channel winds, lifting loose soil and
- 357 fine particles from the exposed areas of the valley floor (Zhang et al., 2018).
- 358 Permafrost has been suggested to reduce the susceptibility of the land surface to deflation
- 359 through ice cementation of mineral particles in soil pores, thereby increasing the threshold wind
- velocity required for sediment entrainment (Bullard et al., 2016). Permafrost is extensively
- developed across the Tibetan Plateau, particularly on the Changtang Plateau (supplementary
- 362 figure 3). However, our winter DSAF data indicate that Changtang Plateau is a DSAF hotspot
- with activation on ~4% of winter days (figures 8(a-b)). We infer that the extremely dry and
- windy conditions on the Changtang Plateau (annual precipitation 200 to 400 mm) lead to
- 365 extremely low soil moisture levels and permafrost characterized by limited pore-ice, making
- deflation of mineral dust still possible in winter (figures 8(c-d)).

4. Conclusions

367

- Dust storms in East Asia affect the health and livelihoods of hundreds of millions of people.
- We present the results of a systematic study of their sources and activation frequency for a
- region spanning 80–130°E and 27–52°N from January 2016 to December 2023 based on skilled
- human analysis of over 420 thousand satellite images. We draw the following conclusions:
- 372 (1) East Asia shows striking seasonal changes in both overall dust source activation frequency
- and in the latitudinal distribution of these events.
- 374 (2) There are two primary dust source regions in East Asia: a southern source region centred
- on the margins of the Taklimakan Desert and a northern source region centred on the valleys
- of the Gobi Desert. The presence of lakes and paleolake remnants in both regions, especially
- in the Taklimakan Desert (e.g., the Lop Nur, and the Tarim River, the Hetain River) promote
- 378 DSAF hotspots.
- 379 (3) The Alashan Plateau (in the southern source region) is dust-active throughout the year. In
- 380 this area and its adjacent regions, dry lakes, such as Gashun Nor, exhibit the highest DSAF,
- followed by oasis areas and croplands along the Hexi Corridor. The sandy deserts in this region
- are much less dust-active and the Chinese Loess Plateau is almost completely inactive as a dust
- 383 source.
- 384 (4) The Tibetan Plateau is not only a sink for windblown dust supplied from elsewhere; it is
- also an active dust source in winter and earliest spring. Here, precipitation patterns, snow cover
- and funnelling of winds through steep river gorges all control activation.
- 387 (5) The Mongolian Plateau (in the northern source region) is a significant dust source in spring.
- 388 Snow cover limits the northernmost extent of dust emissions in February. Vegetation suppresses
- dust emissions across the Mongolian Plateau, particularly in its northeastern region from April
- 390 through May. The bare lands, grasslands and croplands of the region are all susceptible to dust
- 391 source activation. The record-breaking Siberian heatwave of 2020 was associated with a spike
- 392 in DSAF on the Mongolian Plateau over grasslands where livestock overgrazing is well
- 393 documented.

- The seasonal and latitudinal signals in our data, together with the anomaly associated with the
- 395 2020 heatwave, illustrate the power of our data set for quantifying modern dust source
- activation on observed human timescales. Our data also offer a framework to help evaluate past
- 397 variabilities that have undoubtedly occurred on historical and geological timescales and to
- assess future change.

407

Acknowledgements

- 400 The Himawari L1 Gridded data (produced from Himawari-8/9) used in this paper was supplied
- by the P-Tree System, Japan Aerospace Exploration Agency (JAXA). We acknowledge the use
- 402 of the IRIDIS High Performance Computing Facility, and associated support services at the
- 403 University of Southampton, in the completion of this work. We also thank Duo Chan for his
- 404 assistance with IRIDIS. This work was supported by the Natural Environment Research
- 405 Council (studentship NE/S007210/1 to LC through the INSPIRE Doctoral Training
- 406 Programme).

Data availability statement

- 408 The Himawari-8/9 data were obtained from the P-Tree System, operated by the Japan
- 409 Aerospace Exploration Agency (JAXA) (https://www.eorc.jaxa.jp/ptree/). The ECMWF ERA5
- 410 climate reanalysis data were accessed through the Copernicus Climate Change Service Climate
- Data Store (https://cds.climate.copernicus.eu/datasets/). MODIS MCD12C1 Version 6.1 land
- 412 cover data were obtained from the Land Processes Distributed Active Archive Center
- 413 (https://lpdaac.usgs.gov/products/mcd12c1v061/). The livestock data is obtained from the
- National Statistical Office of Mongolia (https://www.1212.mn/en). All data that support the
- 415 findings of this study are included within the article (and any supplementary files).

416 Reference

- 417 Akihiro, S., 2020. Introduction to Himawari-8 RGB composite imagery. Meteorological
- 418 Satellite Center Technical Note 65.
- 419 AlNasser, F., Entekhabi, D., 2024. DustSCAN: A Five Year (2018-2022) Hourly Dataset of
- 420 Dust Plumes From SEVIRI. Sci Data 11, 607.
- 421 Altausen, D., Kai, K., Minamoto, Y., Nakamura, K., Wang, M., Kawai, K., Ohara, K., Noda,
- 422 J., Maki, T., Davaanyam, E., Sugimoto, N., Abdullaev, S., Hofer, J., 2019. Large-scale dust
- event in East Asia, as revealed by the Himawari-8 DUST RGB, lidar network observations,
- 424 and field survey. E3S Web of Conferences 99, 01004.
- 425 An, L., Che, H., Xue, M., Zhang, T., Wang, H., Wang, Y., Zhou, C., Zhao, H., Gui, K., Zheng,
- 426 Y., Sun, T., Liang, Y., Sun, E., Zhang, H., Zhang, X., 2018. Temporal and spatial variations
- in sand and dust storm events in East Asia from 2007 to 2016: Relationships with surface
- 428 conditions and climate change. Sci Total Environ 633, 452-462.
- 429 Banks, J.R., Hünerbein, A., Heinold, B., Brindley, H.E., Deneke, H., Schepanski, K., 2019.
- 430 The sensitivity of the colour of dust in MSG-SEVIRI Desert Dust infrared composite
- imagery to surface and atmospheric conditions. Atmospheric Chemistry and Physics 19,
- 432 6893-6911.
- 433 Bessho, K., Date, K., Hayashi, M., Ikeda, A., Imai, T., Inoue, H., Kumagai, Y., Miyakawa, T.,
- 434 Murata, H., Ohno, T., Okuyama, A., Oyama, R., Sasaki, Y., Shimazu, Y., Shimoji, K., Sumida,
- 435 Y., Suzuki, M., Taniguchi, H., Tsuchiyama, H., Uesawa, D., Yokota, H., Yoshida, R., 2016.

- 436 An Introduction to Himawari-8/9— Japan's New-Generation
- 437 Geostationary Meteorological Satellites. Journal of the Meteorological Society of Japan.
- 438 Ser. II 94, 151-183.
- 439 Bullard, J.E., Baddock, M., Bradwell, T., Crusius, J., Darlington, E., Gaiero, D., Gassó, S.,
- 440 Gisladottir, G., Hodgkins, R., McCulloch, R., McKenna-Neuman, C., Mockford, T.,
- 441 Stewart, H., Thorsteinsson, T., 2016. High-latitude dust in the Earth system. Reviews of
- 442 Geophysics 54, 447-485.
- 443 Chen, Y., Takeuchi, K., Xu, C., Chen, Y., Xu, Z., 2006. Regional climate change and its
- effects on river runoff in the Tarim Basin, China. Hydrological Processes 20, 2207-2216.
- Ciavarella, A., Cotterill, D., Stott, P., Kew, S., Philip, S., van Oldenborgh, G.J., Skalevag, A.,
- Lorenz, P., Robin, Y., Otto, F., Hauser, M., Seneviratne, S.I., Lehner, F., Zolina, O., 2021.
- 447 Prolonged Siberian heat of 2020 almost impossible without human influence. Clim
- 448 Change 166, 9.
- Dong, Z., Lv, P., Qian, G., Xia, X., Zhao, Y., Mu, G., 2012. Research progress in China's Lop
- 450 Nur. Earth-Science Reviews 111, 142-153.
- 451 Du, H., Xue, X., Wang, T., Lu, S., Liao, J., Li, S., Fan, Y., Liu, X., 2022. Modeling dust
- 452 emission in alpine regions with low air temperature and low air pressure A case study
- 453 on the Qinghai-Tibetan Plateau (QTP). Geoderma 422, 115930.
- 454 Ginoux, P., Prospero, J.M., Gill, T.E., Hsu, N.C., Zhao, M., 2012. Global-scale attribution
- of anthropogenic and natural dust sources and their emission rates based on MODIS
- 456 Deep Blue aerosol products. Reviews of Geophysics 50.
- 457 Ginoux, P., Prospero, J.M., Torres, O., Chin, M., 2004. Long-term simulation of global dust
- 458 distribution with the GOCART model: correlation with North Atlantic Oscillation.
- 459 Environmental Modelling & Software 19, 113-128.
- 460 Han, Y., Fang, X., Kang, S., Wang, H., Kang, F., 2008. Shifts of dust source regions over
- 461 central Asia and the Tibetan Plateau: Connections with the Arctic oscillation and the
- westerly jet. Atmospheric Environment 42, 2358-2368.
- 463 Hao, Y., Wang, Z., Xue, L., Lou, S., Ding, K., Qin, Y., Huang, X., 2024. Modeling the Effects
- of Vegetation and Snow on Dust Storm Over the Gobi Desert. Journal of Geophysical
- 465 Research: Atmospheres 129.
- 466 Hennen, M., White, K., Shahgedanova, M., 2019. An Assessment of SEVIRI Imagery at
- 467 Various Temporal Resolutions and the Effect on Accurate Dust Emission Mapping.
- 468 Remote Sensing 11, 918.
- Huang, J., Wang, T., Wang, W., Li, Z., Yan, H., 2014. Climate effects of dust aerosols over
- 470 East Asian arid and semiarid regions. Journal of Geophysical Research: Atmospheres 119.
- Huang, Z., Huang, J., Hayasaka, T., Wang, S., Zhou, T., Jin, H., 2015. Short-cut transport
- path for Asian dust directly to the Arctic: a case study. Environmental Research Letters
- 473 10, 114018.
- 474 Kai, K., Kawai, K., Ito, A., Aizawa, Y., Minamoto, Y., Munkhjargal, E., Davaanyam, E., 2021.
- 475 Dust Hotspot in the Gobi Desert: A Field Survey in April 2019. Sola 17, 130-133.
- 476 Kim, C.-H., Lee, H.-J., 2013. Numerical simulations of Asian dust events: A Lagrangian
- 477 Dust Model and its applications. Asia-Pacific Journal of Atmospheric Sciences 49, 571-
- 478 586.
- 479 Kok, J.F., Adebiyi, A.A., Albani, S., Balkanski, Y., Checa-Garcia, R., Chin, M., Colarco, P.R.,
- 480 Hamilton, D.S., Huang, Y., Ito, A., Klose, M., Li, L., Mahowald, N.M., Miller, R.L., Obiso, V.,
- 481 Pérez García-Pando, C., Rocha-Lima, A., Wan, J.S., 2021. Contribution of the world's main

- 482 dust source regions to the global cycle of desert dust. Atmospheric Chemistry and
- 483 Physics 21, 8169-8193.
- 484 Kok, J.F., Storelvmo, T., Karydis, V.A., Adebiyi, A.A., Mahowald, N.M., Evan, A.T., He, C.,
- Leung, D.M., 2023. Mineral dust aerosol impacts on global climate and climate change.
- 486 Nature Reviews Earth & Environment 4, 71-86.
- 487 Kunkelova, T., Crocker, A.J., Jewell, A.M., Breeze, P.S., Drake, N.A., Cooper, M.J., Milton,
- 488 J.A., Hennen, M., Shahgedanova, M., Petraglia, M., Wilson, P.A., 2022. Dust sources in
- 489 Westernmost Asia have a different geochemical fingerprint to those in the Sahara.
- 490 Quaternary Science Reviews 294, 107717.
- 491 Kunkelova, T., Crocker, A.J., Wilson, P.A., Schepanski, K., 2024. Dust Source Activation
- 492 Frequency in the Horn of Africa. Journal of Geophysical Research: Atmospheres 129.
- 493 Kurosaki, Y., Mikami, M., 2003. Recent frequent dust events and their relation to surface
- 494 wind in East Asia. Geophysical Research Letters 30.
- 495 Kurosaki, Y., Mikami, M., 2004. Effect of snow cover on threshold wind velocity of dust
- 496 outbreak. Geophysical Research Letters 31.
- 497 Lee, J.-J., Kim, C.-H., 2012. Roles of surface wind, NDVI and snow cover in the recent
- 498 changes in Asian dust storm occurrence frequency. Atmospheric Environment 59, 366-
- 499 375
- Lehmkuhl, F., Grunert, J., Hülle, D., Batkhishig, O., Stauch, G., 2018. Paleolakes in the
- 501 Gobi region of southern Mongolia. Quaternary Science Reviews 179, 1-23.
- Lehmkuhl, F., Wolf, D., Boemke, B., Klinge, M., Batkhishig, O., Grunert, J., 2024. Aeolian
- 503 sediments in western Mongolia: Distribution and (paleo)climatic implications.
- 504 Geomorphology 465, 109407.
- 505 Li, F.-R., Zhao, L.-Y., Zhang, H., Zhang, T.-H., Shirato, Y., 2004. Wind erosion and airborne
- 506 dust deposition in farmland during spring in the Horqin Sandy Land of eastern Inner
- 507 Mongolia, China. Soil and Tillage Research 75, 121-130.
- 508 Lim, J.-Y., Chun, Y., 2006. The characteristics of Asian dust events in Northeast Asia
- 509 during the springtime from 1993 to 2004. Global and Planetary Change 52, 231-247.
- Lu, P., Han, J., Li, Z., Xu, R., Li, R., Hao, T., Qiao, G., 2020a. Lake outburst accelerated
- 511 permafrost degradation on Qinghai-Tibet Plateau. Remote Sensing of Environment 249,
- 512 112011.
- Lu, S., Chen, F., Zhou, J., Hughes, A.C., Ma, X., Gao, W., 2020b. Cascading implications
- of a single climate change event for fragile ecosystems on the Qinghai-Tibetan Plateau.
- 515 Ecosphere 11.
- 516 Luo, H., Guan, Q., Pan, N., Wang, Q., Li, H., Lin, J., Tan, Z., Shao, W., 2020. Using
- 517 composite fingerprints to quantify the potential dust source contributions in northwest
- 518 China. Sci Total Environ 742, 140560.
- Nandintsetseg, B., Boldgiv, B., Chang, J., Ciais, P., Davaanyam, E., Batbold, A., Bat-Oyun,
- 520 T., Stenseth, N.C., 2021. Risk and vulnerability of Mongolian grasslands under climate
- 521 change. Environmental Research Letters 16, 034035.
- Nandintsetseg, B., Shinoda, M., 2015. Land surface memory effects on dust emission in
- 523 a Mongolian temperate grassland. Journal of Geophysical Research: Biogeosciences 120,
- 524 414-427.
- 525 Natsagdorj, L., Jugder, D., Chung, Y.S., 2003. Analysis of dust storms observed in
- 526 Mongolia during 1937–1999. Atmospheric Environment 37, 1401-1411.

- 527 Nobakht, M., Shahgedanova, M., White, K., 2021. New Inventory of Dust Emission
- 528 Sources in Central Asia and Northwestern China Derived From MODIS Imagery Using
- 529 Dust Enhancement Technique. Journal of Geophysical Research: Atmospheres 126.
- Prospero, J.M., Ginoux, P., Torres, O., Nicholson, S.E., Gill, T.E., 2002. Environmental
- 531 Characterization of Global Sources of Atmospheric Soil Dust Identified with the Nimbus
- 7 Total Ozone Mapping Spectrometer (Toms) Absorbing Aerosol Product. Reviews of
- 533 Geophysics 40.
- Pye, K., Zhou, L.-P., 1989. Late Pleistocene and Holocene aeolian dust deposition in north
- 535 China and the northwest Pacific Ocean. Palaeogeography, Palaeoclimatology,
- 536 Palaeoecology 73, 11-23.
- Qian, W., Quan, L., Shi, S., 2002. Variations of the dust storm in China and its climatic
- 538 control. Journal of climate 15, 1216-1229.
- Rittner, M., Vermeesch, P., Carter, A., Bird, A., Stevens, T., Garzanti, E., Andò, S., Vezzoli,
- 540 G., Dutt, R., Xu, Z., Lu, H., 2016. The provenance of Taklamakan desert sand. Earth and
- 541 Planetary Science Letters 437, 127-137.
- 542 Schär, C., Lüthi, D., Schiemann, R., 2009. Seasonality and Interannual Variability of the
- 543 Westerly Jet in the Tibetan Plateau Region*. Journal of Climate 22, 2940-2957.
- 544 Schepanski, K., Tegen, I., Laurent, B., Heinold, B., Macke, A., 2007. A new Saharan dust
- source activation frequency map derived from MSG-SEVIRI IR-channels. Geophysical
- 546 Research Letters 34, L18803.
- 547 Shao, Y., Dong, C.H., 2006. A review on East Asian dust storm climate, modelling and
- 548 monitoring. Global and Planetary Change 52, 1-22.
- 549 Shen, Y., Shen, Z., Du, M., WANG, W., 2005. Dust emission over different land surface in
- 550 the arid region of northwest China. Journal of the Meteorological Society of Japan. Ser. II
- 551 83, 935-942.
- 552 Shinoda, M., Kimura, R., Mikami, M., Tsubo, M., Nishihara, E., Ishizuka, M., Yamada, Y.,
- 553 Munkhtsetseg, E., Jugder, D., Kurosaki, Y., 2010. Characteristics of Dust Emission in the
- Mongolian Steppe during the 2008 DUVEX Intensive Observational Period. Sola 6, 9-12.
- 555 Sun, J., Zhang, M., Liu, T., 2001. Spatial and temporal characteristics of dust storms in
- 556 China and its surrounding regions, 1960-1999: Relations to source area and climate.
- Journal of Geophysical Research: Atmospheres 106, 10325-10333.
- 558 Tanaka, T.Y., Sekiyama, T.T., Maki, T., Mikami, M., 2011. The Effects of Snow Cover and Soil
- Moisture on Asian Dust: I. A Numerical Sensitivity Study. Sola 7A, 36-39.
- 560 Wang, R.-D., Li, Q., Zhang, C.-L., Wang, Z.-T., Guo, Z.-L., Chang, C.-P., Li, J.-F., 2021.
- 561 Comparison of dust emission ability of sand desert, gravel desert (Gobi), and farmland in
- 562 northern China. Catena 201, 105215.
- Wang, S., Wang, J., Zhou, Z., Shang, K., 2005. Regional characteristics of three kinds of
- dust storm events in China. Atmospheric Environment 39, 509-520.
- Wang, T., Yan, C.Z., Song, X., Li, S., 2011. Landsat Images Reveal Trends in the Aeolian
- Desertification in a Source Area for Sand and Dust Storms in China's Alashan Plateau
- 567 (1975–2007). Land Degradation & Development 24, 422-429.
- Wang, Y., Jia, J., Lu, H., Lu, C., Xia, D., 2019. Fluvial sediments in the Alagxa Plateau as a
- dust source: iron mineralogical and geochemical evidence. Journal of Arid Land 11, 217-
- 570 227.
- Wu, J., Kurosaki, Y., Shinoda, M., Kai, K., 2016. Regional Characteristics of Recent Dust
- 572 Occurrence and Its Controlling Factors in East Asia. Sola 12, 187-191.

- 573 Xuan, J., Sokolik, I.N., 2002. Characterization of sources and emission rates of mineral
- dust in Northern China. Atmospheric Environment 36, 4863-4876.
- 575 Xuan, J., Sokolik, I.N., Hao, J., Guo, F., Mao, H., Yang, G., 2004. Identification and
- 576 characterization of sources of atmospheric mineral dust in East Asia. Atmospheric
- 577 Environment 38, 6239-6252.
- 578 Yang, J., Chen, S., Ling, Z., Zhang, C., Wang, L., Wang, H., Wang, S., Gao, F., Lizaga, I.,
- Wang, F., Yang, S., Chen, F., 2025. Spatiotemporal evolution of aeolian sedimentary
- 580 landscapes on the southern Tibetan Plateau during the late Quaternary: A review and
- recent advances. Earth-Science Reviews 261, 105035.
- 582 Yu, Y., Kalashnikova, O.V., Garay, M.J., Notaro, M., 2019. Climatology of Asian dust
- 583 activation and transport potential based on MISR satellite observations and trajectory
- analysis. Atmospheric Chemistry and Physics 19, 363-378.
- Yumimoto, K., Kajino, M., Tanaka, T.Y., Uno, I., 2019. Dust Vortex in the Taklimakan Desert
- 586 by Himawari-8 High Frequency and Resolution Observation. Sci Rep 9, 1209.
- Zdanowicz, C., Hall, G., Vaive, J., Amelin, Y., Percival, J., Girard, I., Biscaye, P., Bory, A.,
- 588 2006. Asian dustfall in the St. Elias Mountains, Yukon, Canada. Geochimica et
- 589 Cosmochimica Acta 70, 3493-3507.
- 590 Zender, C.S., Bian, H., Newman, D., 2003. Mineral Dust Entrainment and Deposition
- 591 (DEAD) model: Description and 1990s dust climatology. Journal of Geophysical Research:
- 592 Atmospheres 108.
- 593 Zhang, B., Tsunekawa, A., Tsubo, M., 2008. Contributions of sandy lands and stony
- deserts to long-distance dust emission in China and Mongolia during 2000–2006. Global
- 595 and Planetary Change 60, 487-504.
- 596 Zhang, B., Tsunekawa, A., Tsubo, M., 2015a. Identification of Dust Hot Spots from Multi-
- 597 Resolution Remotely Sensed Data in Eastern China and Mongolia. Water, Air, & Soil
- 598 Pollution 226.
- 599 Zhang, C.L., Li, Q., Shen, Y.P., Zhou, N., Wang, X.S., Li, J., Jia, W.R., 2018. Monitoring of
- 600 aeolian desertification on the Qinghai-Tibet Plateau from the 1970s to 2015 using
- 601 Landsat images. Sci Total Environ 619-620, 1648-1659.
- Zhang, X., Zhou, Q., Chen, W., Wang, Y., Tong, D.Q., 2015b. Observation and modeling of
- 603 black soil wind-blown erosion from cropland in Northeastern China. Aeolian Research
- 604 19, 153-162.

- Zhang, Z., Bird, A., Zhang, C., Dong, Z., 2022. Not all gravel deserts in northern China are
- sources of regionally deposited dust. Atmospheric Environment 273, 118984.
- 607 Zhang, Z., Liang, J., Ji, H., Li, M., Ding, J., Tang, C., Zhang, M., Yu, Z., Cao, X., Tian, P., Ren,
- 608 Y., Zhang, L., 2023. Quantifying Mineral Dust Emissions on the Tibetan Plateau With a
- 609 Modified Dust Source Map. Geophysical Research Letters 51.